

State Space Modeling for Optical Fiber Drawing Process

Serge Tchikanda¹ and Kok-Meng Lee²

¹Sandia National Laboratories, Livermore CA.

²Georgia Institute of Technology, Atlanta, GA.

Abstract— A method for obtaining linear state space models of the drawing process is developed. Traditionally, computational fluid dynamics methods have been used to model the drawing process. Although these models have the potential to provide very accurate details of the flow field, they incorporate thousands of dynamic states which make them unsuitable for both real-time simulations and control design. Experimental data have also been used to construct frequency response models which are suitable for control design. However, they heavily rely on the particular operating conditions for which they were obtained. Furthermore, they are constructed using large lumping techniques based on the information at the boundary and cannot predict large perturbations in the flow field. The objective of this paper is to bridge the gap between the system theoretic modeling techniques of the control engineer and the more physically motivated modeling methods of computational fluid dynamics. The method presented here consists of using the basic conservation laws (mass, momentum, and energy) to describe the mean flow of glass along the axial direction. Then, a linear state space model is obtained by spatially discretizing and linearizing the nonlinear partial differential equations. The resulting state space model incorporates all the relevant inputs and outputs of the system in a multiple-input/multiple-output framework. Furthermore, it lends itself to the application of modern control design techniques. The method is simple to implement since all that is needed is the steady state operating points, which can be computed from computational fluid dynamics simulations.

Keywords— Optical Fiber Drawing, State Space Modeling, Computational Fluid Dynamics.

I. INTRODUCTION

OVER the years, optical fiber technology has come to be recognized as an efficient way to transmit signals in high quality telecommunication systems. The fibers in high quality systems must have uniform diameters, high tensile strength, and yet be economically produced. The latter usually means that fibers must be drawn at high speeds to reduce manufacturing costs. Fiber diameter uniformity affects joint and splice loss, optical transmission characteristics, as well as the refractive index profile. Fiber production with high-tensile strength over the entire fiber length is an important factor for fabrication, installation, and maintenance of fiber cable.

The term *draw process* refers to the formation of an optical fiber from a cylindrical glass rod called *preform*. As shown in Fig. 1 a preform of initial radius, R_p , is gradually fed at a rate, v_p , into a cylindrical furnace and peripherally heated to its *softening* temperature. At that temperature the preform becomes soft and a *tension force* is applied at its lower tip to pull the glass downward resulting in a *necking* shape on the preform. As the glass is drawn down-

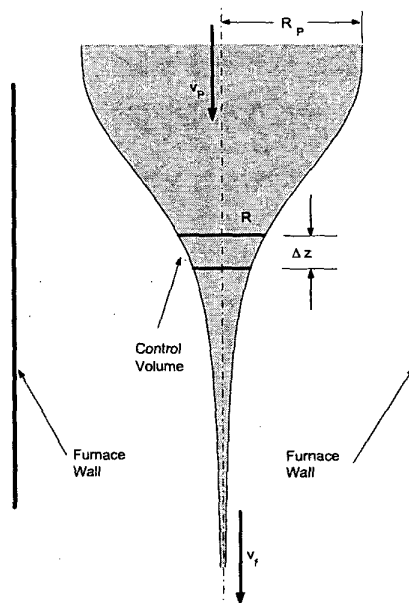


Fig. 1. Longitudinal Section of a Typical Draw Process Configuration

ward at a relatively high speed, v_f , a glass fiber is formed at some location downstream. As the fiber exits the furnace, it enters the cooling stage where it is cooled by the surrounding gas. The fiber is then coated with an organic material to protect its surface from moisture and direct mechanical abrasion. Finally, the coated fiber is wound on spools through a precision winding mechanism.

During the drawing process, the fiber diameter may exhibit significant fluctuations. Such fluctuations result from several factors such as longitudinal variation of the preform diameter, preform feeding rate, unsteady variations of the fiber draw speed, and/or mechanical vibration of the drawing machine. Variations of the furnace temperature will also lead to perturbations of the glass temperature distribution. Since the glass thermophysical properties, such as viscosity and thermal conductivity, are strong functions of temperature, these perturbations will ultimately lead to fiber diameter nonuniformities.

The need to improve the quality of optical fibers and the yield of the drawing process has motivated numerous investigators to model the fiber drawing process in an effort to devise better diameter controllers. Toward this goal,

several researchers (see for example [1]) have attempted to develop accurate models from *Computational Fluid Dynamics (CFD)* to obtain the free surface shape, velocities, and temperature profiles within the glass during the drawing process. These models incorporate thousands of dynamic states and have the potential to provide very accurate two-dimensional models of the flow field. Unfortunately, the large number of states, and the nonlinearity of the equations necessitate large amounts of computational time. Hence, these *CFD* models are unsuitable for both real-time simulations and control design. Computationally more efficient models than the *CFD* models have been developed based on one-dimensional isothermal approximations of the full two-dimensional models [2], [3], [4]. However, since they are isothermal models, they cannot predict fiber diameter perturbations due to temperature fluctuations in the draw process.

Some investigators [5], [6], [7], [8] have also developed frequency response models for the fiber drawing process based on experimental data. Although these frequency response models are suitable for control design, they heavily rely on the particular operating conditions for which they were obtained. Furthermore, they are constructed using large lumping techniques based on the information at the boundary and cannot predict large perturbations in the flow field. As a result they only characterize the input/output relationship of the system and do not reveal any information about internal states like *CFD* models do.

The objective of this paper is to bridge the gap between the system theoretic modeling techniques of the control engineer and the more physically motivated modeling methods of computational fluid dynamics. To achieve this objective, *quasi-one-dimensional* equations describing the mean flow of glass along the axial direction are developed from the basic *conservation laws (mass, momentum, and energy)*. These nonlinear partial differential equations are then discretized and linearized about a steady state operating point to create a finite-dimensional linear state space model, which can be used for control system design.

The model presented here is also different from previous models in that, most control models currently in use are *single-input/single-output (SISO)* in which the draw speed is the only control input to the system. Controlling the fiber diameter using these *SISO* models puts a burden on the draw speed, which in turn results in large variations in draw speeds that adversely affect subsequent process operations such as the application of the coating material. Furthermore, experimental and empirical evidence suggests that the furnace temperature is one of the most influential factors affecting the fiber tension force. Therefore, the dynamics of the draw process must be modeled in a *multiple-input/multiple-output (MIMO)* framework. In other words, an accurate control model of the draw process must include the furnace temperature, preform feed rate, and fiber draw speed as control inputs; and fiber diameter, tension force, and fiber temperature as control outputs. The fiber temperature is monitored because it affects the application of the coating material.

II. DYNAMIC EQUATIONS

The dynamic equations presented in this section are based on the one-dimensional conservation of *mass, momentum, and energy*. They are referred to as the quasi-one-dimensional equations and used to approximate the full two dimensional equations. In the quasi-one-dimensional approximation the flow is predominantly in the axial direction. Although there is some motion in the radial direction, the radial momentum equation is negligible. The approximation is reasonable at steady state especially in the *draw-down* region where most of the fiber formation occurs.

To apply the conservation laws to develop the dynamic equations, one must identify an appropriate *control volume*, a region of space bounded by a *control surface* through which energy and matter may pass. In cylindrical coordinates, a suitable control volume is an infinitesimal cylinder of radius R , cross sectional area $a = \pi R^2$, and length Δz as shown in Fig. 1. The axial velocity and axial temperature at the center of the control volume are v and T , respectively. Stated in the context of the differential control volume shown in Fig. 1, the conservation of mass, momentum, and energy describing the mean flow of glass along the axial direction are given by

$$\frac{\partial a}{\partial t} + \frac{\partial}{\partial z} (av) = 0, \quad (1)$$

$$\rho \left[\frac{\partial}{\partial t} (av) + \frac{\partial}{\partial z} (av^2) \right] = \frac{\partial}{\partial z} \left[a \left(3\mu \frac{\partial v}{\partial z} + \kappa \gamma \right) \right] + \rho g a, \quad (2)$$

$$\rho c_p \left[\frac{\partial}{\partial t} (aT) + \frac{\partial}{\partial z} (avT) \right] = \frac{\partial}{\partial z} \left(ka \frac{\partial T}{\partial z} \right) - 2\pi R \left(q''_{rad} + q''_{conv} \right) + a \left(3\mu \frac{\partial v}{\partial z} + \kappa \gamma \right) \frac{\partial v}{\partial z}, \quad (3)$$

where t is time and z is the axial distance; ρ , μ , κ , γ , and g are the density, dynamic viscosity, surface curvature, surface tension coefficient, and gravitational acceleration, respectively; and c_p and k are the specific heat and thermal conductivity, respectively. The *convective* and *radiative heat fluxes* at the glass surface are given by

$$q''_{conv}(z) = h(z) [T(z) - T_\infty], \quad (4)$$

$$q''_{rad}(z, t) = \sigma \varepsilon T^4 - q(t) q''_{fur}(z), \quad (5)$$

where h is the heat transfer coefficient at the surface, T_∞ is the surrounding gas temperature, ε is the glass "*effective*" emissivity, $\sigma = 5.67051 \times 10^{-8} \text{ W m}^{-2} \text{ K}^{-4}$ is the *Stefan-Boltzmann constant*, and $q(t) q''_{fur}(z)$ represents the heat flux leaving the furnace that is incident on the glass surface. The spatial distribution of the furnace heat flux, $q''_{fur}(z)$, is obtained from [1] and its intensity is given by the following differential equation:

$$\tau_q \dot{q}(t) + q(t) = K_q I_q(t), \quad (6)$$

where I_q is the input current to the furnace, and τ_q and K_q are the furnace time constant and gain, respectively.

To simplify the presentation and utilization of the solutions, the conservation equations are rewritten in dimensionless form. They are also transformed to a generalized curvilinear coordinate, $\xi = \xi(z)$, and cast into the vector form. The nondimensionalizing procedure may be done by normalizing the relevant variables with appropriate scales and arranging them into suitable *dimensionless groups*. Thus by identifying the following scales:

$$a \sim R_P^2, v \sim v_f, z \sim R_P, t \sim R_P/v_f, \kappa \sim 1/R_P, \\ T \sim T_m, \mu \sim \mu_m, k \sim k_m, c_p \sim c_{p,m}, \gamma \sim \gamma_m,$$

where the subscript "m" denotes value at the *melting point*, the conservation equations are rewritten as

$$E \left(J \frac{\partial Q}{\partial t} + \frac{\partial F}{\partial \xi} \right) = \frac{\partial}{\partial \xi} \left(\Gamma \frac{\partial Q}{\partial \xi} \right) + S, \quad (7)$$

where Q , F , and S , are the *state vector*, *convective flux vector*, and *source vector*, respectively, given by

$$Q = [a \quad v \quad T]^T, \\ F = [av \quad av^2 \quad avT]^T,$$

$$S = \begin{bmatrix} 0 \\ s_1 a \xi + a s_2 \\ a^{1/2} \left\{ s_5 T^4 + s_6 q(t) q''_{fur} + s_7 (T - T_\infty) \right\} + \\ a (s_3 v_\xi^2 + s_4 v_\xi) \end{bmatrix},$$

where

$$s_1 = \frac{\kappa \gamma}{ReCa}, \quad s_2 = \frac{\partial s_1}{\partial \xi} + \frac{\xi^{-1}}{Fr}, \quad s_3 = \frac{3\mu\xi_z}{ReEc^{-1}}, \quad s_4 = s_1 Ec, \\ s_5 = -\frac{2\sqrt{\pi}\sigma\varepsilon T_m^3}{\rho v_f \xi_z c_{p,m}}, \quad s_6 = \frac{2\sqrt{\pi}}{\rho v_f T_m \xi_z c_{p,m}}, \quad s_7 = -\frac{2\sqrt{\pi}h(z)}{\rho v_f \xi_z c_{p,m}}.$$

The matrices E , J , and Γ are given by

$$E = \text{diag} (1, 1, c_p), \quad J = \frac{1}{\xi_z} \begin{bmatrix} 1 & 0 & 0 \\ v & a & 0 \\ T & 0 & a \end{bmatrix}, \\ \Gamma = \text{diag} \left(0, \frac{3a\mu\xi_z}{Re}, \frac{ak\xi_z}{Pe} \right) = \text{diag} (0, \Gamma_2, \Gamma_3).$$

The dimensionless groups Re , Pe , Fr , Ec , and Ca are the *Reynolds*, *Peclet*, *Froude*, *Eckert*, and *Capillary* numbers, respectively, defined by

$$Re = \frac{\rho v_f R_P}{\mu_m}, \quad Pe = \frac{v_f R_P}{k_m / \rho c_{p,m}}, \quad Fr = \frac{g R_P}{v_f^2}, \\ Ec = \frac{v_f^2}{c_{p,m} T_m}, \quad Ca = \frac{\mu_m v_f}{\gamma_m}.$$

III. BOUNDARY CONDITIONS

At the inflow, the preform diameter is constant and the axial velocity is equal to the preform feed rate, $v_P(t)$, which is obtained from a motor described by

$$\tau_P \dot{v}_P(t) + v_P(t) = K_P V_P(t), \quad (9)$$

where V_P is the input voltage to the motor, and τ_P and K_P are the motor time constant and gain, respectively. At the inflow the *conductive* heat flux is assumed constant ($\partial^2 T / \partial z^2 = 0$). As a result, the inflow temperature is extrapolated from the interior domain of the glass.

The outflow cross sectional area is obtained from the *continuity* equation given by Eq. (1). Thus,

$$\frac{\partial}{\partial t} \left(\frac{a}{\xi_z} \right) = r_1 \equiv -\frac{\partial}{\partial \xi} (av). \quad (10)$$

The outflow velocity is equal to the fiber draw speed, $v_f(t)$, obtained from a motor described by

$$\tau_f \dot{v}_f(t) + v_f(t) = K_f V_f(t), \quad (11)$$

where V_f is the input voltage to the motor, and τ_f and K_f are the motor time constant and gain, respectively. The outflow temperature is obtained from the conservation of energy requirement. Thus,

$$c_p \left(\frac{aT}{\xi_z} \right)_t = r_3 \equiv \left(\Gamma_3 T_\xi \right)_\xi - c_p (avT)_\xi + a (s_3 v_\xi^2 + s_4 v_\xi) \\ + a^{1/2} \left[s_5 T^4 + s_6 q(t) q''_{fur}(z) + s_7 (T - T_{\infty,m}) \right], \quad (12)$$

where the subscripts "t" and "ξ" denote differentiations.

IV. STATE SPACE MODEL

In Sections II and III, the conservation equations and boundary conditions describing the dynamics of the system were developed, respectively. In this Section, a *state space* form suitable for the application of modern control design techniques is introduced. This is achieved by linearizing and spatially discretizing the conservation equations, which are rewritten here as

$$N \frac{\partial Q}{\partial t} = \mathcal{R}(Q, q), \quad (13)$$

where the residual vector, \mathcal{R} , is defined as

$$\mathcal{R} \equiv \frac{\partial}{\partial \xi} \left(\Gamma \frac{\partial Q}{\partial \xi} \right) - E \frac{\partial F}{\partial \xi} + S, \quad (14)$$

and the matrix $N = EJ$.

To discretize the conservation equations, a one-dimensional grid along the axial coordinate is constructed on the solution domain. The grid points are numbered using the index i with $1 \leq i \leq I$, where I is the maximum number of grid points. The inflow boundary is located at $i = 1$ whereas the outflow is at $i = I$. The residual vector is discretized using a *third order upwind flux difference*

method [9] for the convective flux vector, and the *second order central difference* method [10] for the *diffusion* term and source term vector. Thus,

$$\begin{aligned} \mathcal{R}_i \approx & \Gamma_{i+1/2} (Q_{i+1} - Q_i) - \Gamma_{i-1/2} (Q_i - Q_{i-1}) \\ & + \frac{1}{3} E_i \left[\Omega_{i+1/2} (Q_{i+1} - Q_i) - \Omega_{i-1/2} (Q_i - Q_{i-1}) \right] \\ & - \frac{1}{2} E_i \left[F(Q_{i+1}) - F(Q_{i-1}) \right] + S_i. \end{aligned} \quad (15)$$

where $\Omega = \partial F / \partial Q$ is the Jacobian matrix of the convective flux vector. The discrete residual vector in Eq. (15) can be linearized using a truncated *Taylor* series about some steady state vector, Q , and heat flux, q , to give

$$N_i \delta \dot{Q}_i = \alpha_i \delta Q_{i-1} + \beta_i \delta Q_i + \varphi_i \delta Q_{i+1} + \omega_i \delta q, \quad (16)$$

where δQ and δq are small perturbations about some steady state, and the coefficient matrices are given by

$$\alpha_i = \frac{\partial \mathcal{R}_i}{\partial Q_{i-1}}, \quad \beta_i = \frac{\partial \mathcal{R}_i}{\partial Q_i}, \quad \varphi_i = \frac{\partial \mathcal{R}_i}{\partial Q_{i+1}}, \quad \omega_i = \frac{\partial S_i}{\partial q}.$$

The residual vector at the outflow boundary is

$$\mathcal{R}_I \equiv \begin{bmatrix} r_{1,I} \\ -v_I + K_f V_f \\ r_{3,I} \end{bmatrix}, \quad (18)$$

where the residual components, $r_{1,I}$ and $r_{3,I}$ are obtained from Eqs. (10) and (12) using second order one-sided differences. Upon linearization of the residual vector, \mathcal{R}_I , the following equation at the outflow boundary is obtained:

$$\begin{aligned} N_I \delta \dot{Q}_I = & \psi_I \delta Q_{I-3} + \phi_I \delta Q_{I-2} + \alpha_I \delta Q_{I-1} \\ & + \beta_I \delta Q_I + \omega_I \delta q + \theta K_f V_f, \end{aligned} \quad (19)$$

where

$$N_I = \frac{1}{\xi_z} \begin{bmatrix} 1 & 0 & 0 \\ 0 & \tau_f \xi_z^{-1} & 0 \\ c_{p,I} T_I & 0 & c_{p,I} a_I \end{bmatrix}, \quad \theta = \begin{bmatrix} 0 \\ 1 \\ 0 \end{bmatrix},$$

$$\psi_I = \frac{\partial \mathcal{R}_I}{\partial Q_{I-3}}, \quad \phi_I = \frac{\partial \mathcal{R}_I}{\partial Q_{I-2}}, \quad \alpha_I = \frac{\partial \mathcal{R}_I}{\partial Q_{I-1}}, \quad \beta_I = \frac{\partial \mathcal{R}_I}{\partial Q_I}.$$

The change in inflow state vector, δQ_1 , is expressed as

$$\delta Q_1 = 2W_1 \delta Q_2 - W_1 \delta Q_3 + \theta \delta v_P, \quad (20)$$

where $W_1 = \text{diag}(0, 0, 1)$.

Combining Eqs. (6), (9), (16), (19), and (20), the system state equation can be rewritten as

$$M \dot{x} = A_1 x + B_1 u, \quad (21)$$

where the *global state vector* x and the *input vector* u are defined by

$$\begin{aligned} x &= \left[\delta v_P \quad \delta q \quad \delta Q_2^T \quad \cdots \quad \delta Q_i^T \quad \cdots \quad \delta Q_I^T \right]^T, \\ u &= \left[V_P \quad I_q \quad V_f \right]^T. \end{aligned}$$

The matrices M , A_1 , and B_1 are given by

$$M = \text{blockdiag} \left(\tau_P, \tau_q, N_2, \cdots, N_i, \cdots, N_I \right),$$

$$A_1 = \begin{bmatrix} -1 & 0 & 0_{1 \times 3} & 0_{1 \times 3} & \cdots & \cdots \\ 0 & -1 & 0_{1 \times 3} & 0_{1 \times 3} & \cdots & \cdots \\ \alpha_2 \theta & \omega_2 & \bar{\beta}_2 & \bar{\varphi}_2 & 0_{3 \times 3} & \cdots \\ 0_{3 \times 1} & \omega_3 & \alpha_3 & \beta_3 & \varphi_3 & \cdots \\ & & \ddots & \ddots & \ddots & \\ \vdots & \vdots & & \alpha_i & \beta_i & \varphi_i \\ \vdots & \vdots & & \ddots & \ddots & \ddots \\ 0_{3 \times 1} & \omega_I & \cdots & \psi_I & \phi_I & \alpha_I \quad \beta_I \quad \varphi_{I-1} \end{bmatrix},$$

$$B_1 = \begin{bmatrix} K_P & 0 & 0 \\ 0 & K_q & 0 \\ 0_{3 \times 1} & 0_{3 \times 1} & 0_{3 \times 1} \\ \vdots & \vdots & \vdots \\ 0_{3 \times 1} & 0_{3 \times 1} & 0_{3 \times 1} \\ 0_{3 \times 1} & 0_{3 \times 1} & \theta K_f \end{bmatrix},$$

where $\bar{\beta}_2 = \beta_2 + 2\alpha_2 W_1$ and $\bar{\varphi}_2 = \varphi_2 - \alpha_2 W_1$.

Eq. (21) is the linear state-variable form of the dynamic equations. To complete the state space representation of the system, an *output equation* must be developed. The outputs of the system are the fiber cross-sectional area (from which the fiber diameter can be determined), the fiber tension force, and the fiber temperature. In dimensionless form, the fiber tension force is given by

$$f = a \left(3\mu \xi_z v_\xi + \kappa \gamma C a^{-1} \right). \quad (22)$$

Using a second-order backward difference for the velocity gradient at the outflow boundary¹, Eq. (22) is discretized and linearized as

$$\delta f_I = c_1 \delta Q_I + c_2 \delta Q_{I-1} + c_3 \delta Q_{I-2}, \quad (23)$$

where the vectors c_1 , c_2 , and c_3 are obtained in an obvious manner. Denoting the *output vector* by

$$y = \left[\delta a_I \quad \delta f_I \quad \delta T_I \right]^T,$$

the complete state space representation of the dynamic system is expressed as

$$\begin{aligned} \dot{x} &= Ax + Bu \\ y &= Cx + Du \end{aligned} \quad (24)$$

where the matrices A , B , C , and D are given by

$$\begin{aligned} A &= M^{-1} A_1, \quad B = M^{-1} B_1, \quad D = 0_{3 \times 3} \\ C &= \begin{bmatrix} 0_{1 \times 3} & \cdots & 0_{1 \times 3} & \cdots & 0_{1 \times 3} & 1 & 0_{1 \times 2} \\ 0_{1 \times 3} & \cdots & 0_{1 \times 3} & c_3 & c_2 & c_1 & \\ 0_{1 \times 3} & \cdots & 0_{1 \times 3} & \cdots & 0_{1 \times 3} & 0_{1 \times 2} & 1 \end{bmatrix}. \end{aligned}$$

¹If it is assumed that the final fiber diameter is attained at the outflow boundary and the tension force is measured there.

V. RESULTS AND DISCUSSIONS

In this Section, some results of the state space modeling method developed in Section IV are presented. The number of grid points was $I = 50$ and all parameters such as preform shape, furnace configuration, thermophysical properties, and dimensionless groups are all obtained from [1] and will not be reproduced here due to lack of space. The steady state operating points used in the linearization procedure were obtained from nonlinear *CFD* simulations [1]. The *CFD* simulations provide the steady state vector, Q , about which the linearization procedure is performed.

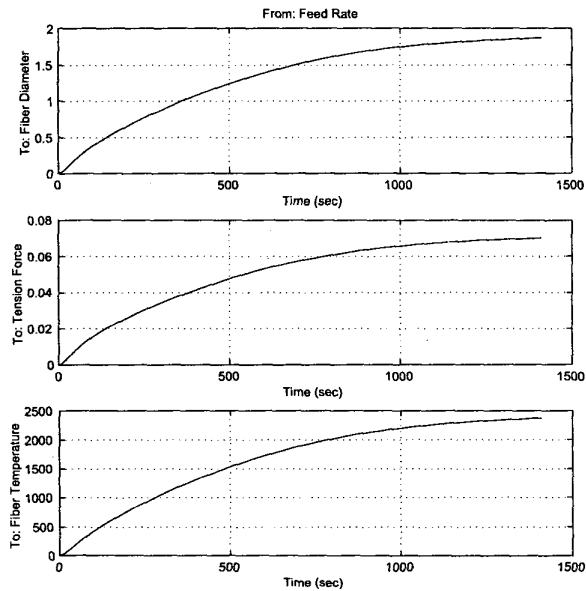


Fig. 2. Responses to a Step Change in Feed Rate Input Voltage.

The unit step responses, with zero initial conditions, are shown in Figs. 2, 3, and 4 in dimensionless form according to the prescriptions in Section II. The fiber diameter; tension force, and temperature responses to a unit step change in feed rate input voltage are shown in Fig. 2. These responses exhibit relatively long rise times and settling times, indicating that the feed rate has a slow effect on the draw process. Many investigators [3], [4], and [5] in the past have neglected the effects of the furnace heat input in their control models. As shown in Fig. 3, the responses to a step change in the furnace heat input current exhibit fast rise times and settling times and some overshoot. Therefore, the dynamics resulting from the furnace heat input cannot be neglected. It has been shown experimentally [5] that the draw speed is the most influential factor affecting the fiber diameter. This is verified in the top-most plot in Fig. 4, as a unit step change in draw speed input voltage produces the most change in fiber diameter compared to those in Figs. 2 and 3. We also see in Fig. 4 that as the draw speed increases, the fiber diameter decreases. This is a direct result of the conservation of mass. That is, high

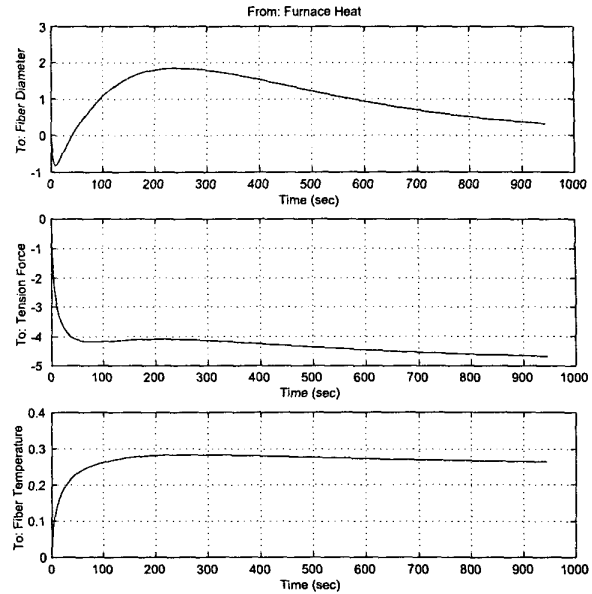


Fig. 3. Responses to a Step Change in Furnace Heat Input Current.

speeds result in small cross sectional areas.

The step responses provide useful information about the system in the time domain. In addition to information in the time domain, information in the frequency domain is also of interest. Fig. 5 shows the singular values plots of the system. These plots give us insights on the magnitude of the open loop ratios between the outputs and the inputs of the system. The frequency response shows high gains at low frequencies indicating the ability of the system to track reference inputs at steady state. We also note a high *roll-off* at high frequencies, which reveals the ability of the system to attenuate high frequency noise.

To validate the linear model, the fiber diameter response of the nonlinear *CFD* model developed in [1] is compared with the linear state space model. It is seen in Fig. 6 that the linear model shows reasonable agreement with the nonlinear *CFD* model.

VI. CONCLUSIONS

A method for obtaining linear state space models of the draw process was developed. The method provides a linear model that can be used for control applications. The method consists of using the basic conservation laws (mass, momentum, and energy) to derive quasi-one-dimensional dynamic equations, which describe the mean flow of glass along the axial direction. The dynamic equations are then spatially discretized and linearized to obtain a linear state space model. Since the state space model is a linearized representation of the nonlinear model, it is valid near one operating point. If the operating condition changes, a new model must be developed. This is not a problem, because the new model is easily computed from new steady state

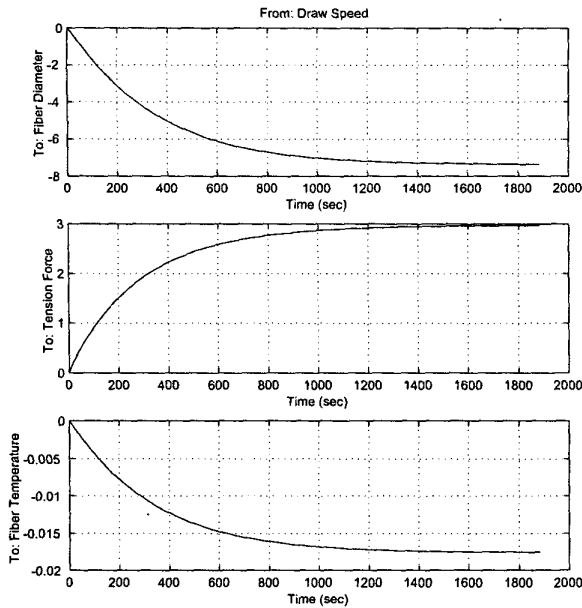


Fig. 4. Responses to a Step Change in Draw Speed Input Voltage

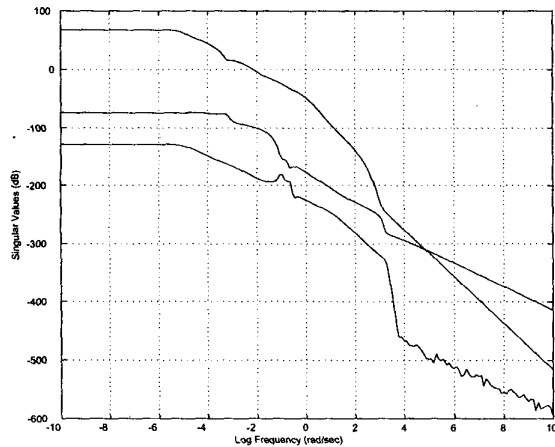


Fig. 5. Singular Values Plots

data from *CFD* simulations. It is instructive to note that the linear model is not guaranteed to be stable around other operating points. This is not a severe limitation in optical fiber control system design since the major concern here is to regulate the outputs about a particular operating point rather than to track reference commands.

Although the method presented here provides an accurate efficient way to obtain state space models suitable for modern control design, it can be improved by considering the effects of time delays that might arise due to physical and/or computational limitations. Furthermore, the method provides nominal models which are approximations to the actual system. In order to guarantee that

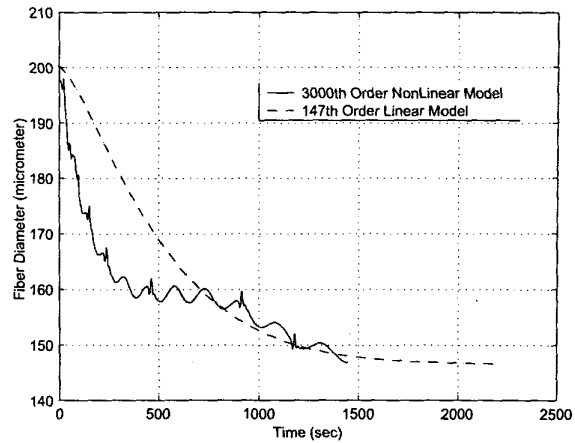


Fig. 6. Fiber Diameter Responses Obtained from Nonlinear CFD and Linear State Space Models

the compensators designed on the basis of plant nominal dynamics or nominal models will result in stable feedback control system, the control engineer must be equipped with models that capture the uncertainty structure of the system. Therefore, the model uncertainty structure should also be accounted for. These issues are currently being investigated by the authors and will be addressed in future papers.

ACKNOWLEDGMENTS

The authors would like to thank Dr. Zhi Zhou and Dr. Siu-Ping Hong both of Lucent Technologies for their technical inputs and financial support for the research.

REFERENCES

- [1] S. W. Tchikanda, *Modeling for High-Speed High-Strength Precision Optical Fiber Drawing*. PhD thesis, The Georgia Institute of Technology, May 2001.
- [2] C. Thompson and A. Mulpur, "Fluid dynamic instabilities in drawn fibers," *Mat. Res. Soc. Symp. Proc.*, vol. 172, 1990.
- [3] A. Mulpur and C. Thompson, "Modal diameter control of linear isothermal optical fibers," in *Second IEEE Conference on Control Applications*, (Vancouver, B.C.), p. 433, September 1993.
- [4] A. Mulpur and C. Thompson, "Nonlinear control of optical fiber diameter variations," in *Proceedings of the American Control Conference*, (Baltimore MD), p. 3528, June 1994.
- [5] D. M. Smithgall, "Application of optimization theory to the control of the optical fiber drawing process," *Bell Sys. Tech. J.*, vol. 58, no. 6, p. 1425, 1979.
- [6] Z. Zhu, G. Dai, and T. Yu, "An optical fiber drawing self-tuning control system," in *Proceedings of the IFAC/IFORS Symposium on Identification and System Parameter Estimation*, (Beijing), p. 1291, 1988.
- [7] K. Imoto, M. Sumi, G. Toda, and T. Saganuma, "Optical fiber drawing method with gas flow controlling system," *Journal of Lightwave Technology*, vol. 7, no. 1, pp. 115-121, 1989.
- [8] S. Milinkovic, R. Aleksic, D. Mitrakovic, and A. Sadibasic, "Characterisation of the optical fibre drawing process," *Glass Technology*, vol. 34, no. 4, pp. 148-153, 1993.
- [9] S. E. Rogers and D. Kwak, "Upwind differencing scheme for the time-accurate incompressible navier-stokes equations," *AIAA Journal*, vol. 28, pp. 253-262, February 1990.
- [10] J. C. Tannehill, D. A. Anderson, and R. H. Fletcher, *Computational Fluid Mechanics and Heat Transfer*. Taylor Francis, 2nd ed., 1997.